Capillarity

Vol. 12, No. 1, p. 6-16, 2024

Original article

Understanding the post-frac soaking process in multi-fractured shale gas-oil wells

Boyun Guo*, Philip Wortman

Department of Petroleum Engineering, Energy Institute of Louisiana at Lafayette, Lafayette 70503, USA

Keywords:
Horizontal well
fracturing
soaking
imbibition
mathematical model
shale gas and oil

Cited as:
Guo, B., Wortman, P. Understanding the post-frac soaking process in multi-fractured shale gas-oil wells. Capillarity, 2024, 12(1): 6-16.
https://doi.org/10.46690/capi.2024.07.02

Abstract:
Multi-stage hydraulic-fracturing horizontal wells has revolutionized today's oil and gas industry. Post-frac fluid soaking is essential for improving productivity of shale oil-gas wells. Optimization of soaking time is an open problem to solve in the petroleum industry. Understanding the post-frac soaking process is vitally important for solving the puzzle. Analytical solutions were developed in this study to describe the spontaneous imbibition processes in shale matrix and shale cracks during fluid soaking. Solutions show that the imbibition distance is directly proportional to the square root of imbibition time and the imbibition velocity is inversely proportional to the square root of imbibition time. The rate of spontaneous imbibition in shale cracks is much faster than that in shale matrix. Therefore, the optimum time for post-frac fluid soaking was further analyzed on the basis of the imbibition in shale cracks only. The solution was combined with pressure fall-off data to formulate a mathematical method for predicting the post-frac fluid soaking time required for the fluid to reach the mid-point between two adjacent hydraulic fractures. A case study with Tuscaloosa Marine Shale data suggests that the front of fluid imbibition should propagate 4 meters in 2 weeks and to 6 meters in 4 weeks. These numbers may be considered as the optimum times of post-frac fluid imbibition if the shale swell effect is negligible. Future research should quantify the effects of shale swelling on spontaneous imbibition so that the information can be incorporated in the soaking model to fully describe the imbibition process for better prediction of well productivity.

1. Introduction

More than 50% of fracturing fluid is retained in shale formation after flow-back. Shale gas wells with high volume of water retention are normally the wells with high production rates. Ehlig-Economides and Economides (2011) inferred that the retained water should work as proppant to keep the induced and natural fractures open and thus maintain fracture conductivity. A great number of researchers have studied this phenomenon in the past. A commonly accepted theory is that the water which soaks into shales results in increased shale permeability and, therefore, promotes gas production rate.

Fluid soaking in shales is due to spontaneous imbibition, which is a natural phenomenon in porous media. Cai and Yu (2012) summarized the research development of the imbibition theory and analyzed previously existing models. Early studies targeted shale field development. Dutta et al. (2012) investigated quantification of fracturing fluid migration due to spontaneous imbibition in fractured tight formations. A great amount of effort has been made to enhance the fluid soaking efficiency to increase gas well production after hydraulic fracturing, mostly on promoting spontaneous fluid imbibition. Cai et al. (2014) presented a generalized model for spontaneous imbibition based on Hagen-Poiseuille flow in tortuous capillaries with variably shaped apertures. Crafton and Noe (2013) reported that some wells received productivity loss by shutting-in the well after fracturing. This was also observed by Yaich et al. (2015) and confirmed by Yan et al. (2015) in their experimental investigations. The effect was attributed to the influence of surfactant additives. Shen

Yandy Scientific Press

*Corresponding author.
E-mail address: boyun.guo@louisiana.edu (B. Guo); philip.wortman1@louisiana.edu (P. Wortman).

Received February 11, 2024; revised March 1, 2024; accepted March 22, 2024; available online March 26, 2024.

et al. (2016) conducted a comparative study of marine and continental shale formations for water imbibition of shale and its potential influence on shale gas recovery.

Habibi et al. (2015) reported the advances in understanding the wettability of tight oil formations. Spontaneous imbibition processes in shale oil reservoirs have been studied in recent years, mainly focusing on laboratory experiments, theoretical analysis, and numerical simulations (Cai, 2021). A numerical study was performed on shale oil reservoirs by Wang et al. (2022). Their result shows that, with the increase of shut-in time, both the initial oil production and cumulative oil production volume increase rapidly at first and then level off. The shut-in time corresponding to the inflection point in the trend of cumulative production increment was selected as the optimal shut-in time. Shaibu and Guo (2021) provided a decade literature review of the dilemma of fluid soaking in hydraulically fractured horizontal shale well prior to flowback.

Cai et al. (2023) provides a summary of the most recent advances in the studies of capillary behavior in shale gas/oil reservoirs, showing the challenge in modeling of the spontaneous imbibition due to the complex imbibition mechanism. Owing to the multi-influencing factors such as petrophysical properties of shales and fluid properties, it is difficult to understand thoroughly the microscopic and macroscopic flow mechanisms in spontaneous imbibition processes.

Although numerous researchers have studied the spontaneous imbibition behavior in shale gas/oil reservoirs, very limited progress has been made in predicting the optimum time of post-frac soaking. This shortcoming of the previous research motivated our new investigations. Focusing on the average properties of shale matrix, shale cracks, and fracturing fluids, this study developed analytical solutions to describe the spontaneous imbibition processes in shale matrix and shale cracks during fluid soaking. The optimum time for post-frac fluid soaking was analyzed based on the imbibition in shale cracks. A case study is presented by combining the solutions with a pressure fall-off data set for estimating the post-frac fluid soaking time required for the fluid to reach the mid-point between two adjacent hydraulic fractures.

2. Physical process of soaking

The post-frac fluid soaking process is promoted by spontaneous imbibition processes induced by capillary force, resisted by viscous friction force, promoted/demoted by gravitational force depending on orientation of the motion relative to gravity, and effected by swelling of clayey materials.

On the basis of the accumulated knowledge of researchers in the past two decades, the post-frac fluid soaking process is described as follows.

1) Fracturing fluid imbibes into rock matrix driven by capillary force and resisted by viscous force. The imbibition depth can be described by the following equation (see Appendix A for derivation):

$$x = \sqrt{\frac{\sigma k_{rw} k \varphi \cos\theta}{245.25 \mu_w r_c} t} \tag{1}$$

Table 1. Formation and fluid properties in the TMS shale (Lu et al., 2015).

Parameter	Value	Unit
Shale porosity	0.02	-
Absolute permeability	0.000051	mD
Equivalent pore diameter	2.088E-05	cm
Relative permeability	1	-
Interfacial tension	60	Dyne/cm
Contact angle	80	degree
Viscosity	1	cp

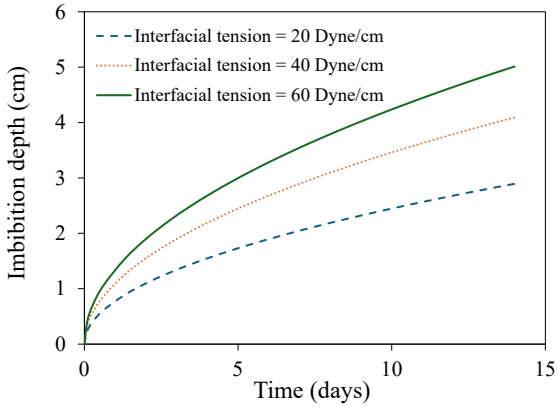

Fig. 1. Model-predicted spontaneous water imbibition into the matrix of TMS shale for different interfacial tensions.

where x is imbibition depth in cm, σ in interfacial tension in Dyne/cm, k_{rw} is the relative permeability to the wetting phase, k is the absolute permeability in Darcy, φ is porosity in fraction, θ is the contact angle measured in the wetting phase in degree, μ_w is wetting phase viscosity in cp, r_c is the equivalent capillary radius in cm and t is imbibition time in s. Eq. (1) is very similar to Handy's (1960) solution where the relative permeability was assumed to be wetting phase saturation. The imbibition velocity (v) is expressed by:

$$v = \frac{\mathrm{d}x}{\mathrm{d}t} = \sqrt{\frac{\sigma k_{rw} k \varphi \cos\theta}{981 \mu_w r_c t}} \tag{2}$$

Table 1 presents some data for the Tuscaloosa marine shale (TMS). The equivalent pore size was estimated by the correlation of Kolodzie Jr (1980) modified by Pittman (1992). The value of relative permeability is set to unity because of single-phase flow in the cracks during fluid soaking period. Calculated trends of spontaneous imbibition by Eq. (1) are presented in Figs. 1 and 2 for various interfacial tension and contact angles. It is seen from these curves that the spontaneous imbibition into the shale is extremely low. The imbibition depth in 14 days is within 10 cm, even with favorable fluid properties (high interfacial tension and low contact angle).

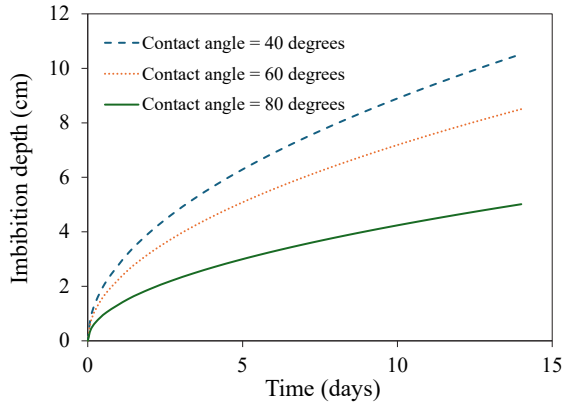

Fig. 2. Model-predicted spontaneous water imbibition into the matrix of TMS shale for different contact angles.

Table 2. Crack and fluid properties for sensitivity analysis (Guo et al., 2020).

Parameter	Value	Unit
Crack width	0.00002	cm
Interfacial tension	60	Dyne/cm
Contact angle	80	degree
Viscosity	1	cp

2) Fracture pressure induces shale cracks initiated from fractures. Guo et al. (2020) defined and illustrated the difference between fractures and cracks. The 'fractures' are defined as vertical fractures that propagate horizontally orthogonal to the horizontal wellbore induced by fracking and 'cracks' are horizontal fractures which propagate from the induced vertical fractures. As depicted in Fig. 3, the net pressure defined as the fracture fluid pressure minus the minimum formation stress creates the same additional compressive stress inside the shale layers. Because the values of Young's modulus of shale layers are different, the same stress will create different strains in different layers. Therefore, the shale layers will deform differently, creating different displacements at the fracture face, resulting in shear failure, or cracks, at the interfaces of shale layers. Many researchers, including Guo et al. (2020), have shown evidence of shale crack formation due to the change of surrounding pressure. In this paper, 'fractures' are defined as vertical fractures that propagate horizontally orthogonal to the horizontal wellbore induced by fracking and 'cracks' are horizontal fractures which propagate from the induced vertical fractures.
3) Fracturing fluid imbibes into the cracks due to capillary force and resisted by viscous force. The crack surfaces are lubricated by the imbibed hydraulic fracturing fluid and promote extension of the cracks. The imbibition depth along the crack can be described by the following equation (see Appendix A for derivation):

$$x = \sqrt{\frac{100w\sigma\cos\theta}{\mu_w}t} \tag{3}$$

where w is crack width in cm. The imbibition velocity is expressed by:

$$v = \frac{\mathrm{d}x}{\mathrm{d}t} = \sqrt{\frac{25w\sigma\cos\theta}{\mu_w t}} \tag{4}$$

Using the data in Table 2, the trends of spontaneous imbibition given by Eq. (3) are plotted in Figs. 4-6 for different values of interfacial tension, contact angle, and crack width. It is informed from these curves that the spontaneous imbibition into a crack is more than 80 cm in 14 days, which is much higher than that into the shale matrix shown in Figs. 1 and 2. Therefore, the spontaneous imbibition into cracks, rather than in shale matrix, should be considered as a priority in the fluid soaking process.
4) Clay swells and plugs the shale pores and cracks. As the fluid imbibition progresses, the clayey minerals inside the shale and at the surfaces of cracks begin to swell and partially plug the pore and the induced cracks. Although tons of literature have demonstrated the negative effect of clay-swelling on fluid transfer in porous media, it is extremely difficult, if not impossible, to quantitatively describe the time-dependent flow resistance to fluid flow in real cracks. This effect reduces the effectiveness of long-time fluid soaking for well productivity improvement.

3. Termination of soaking process

Previous investigations indicate that there is an optimum time to stop the fluid soaking to improve well productivity (Crafton and Noe, 2013; Yaich et al., 2015; Yan et al., 2015). Guo et al. (2020) assumed that the productivity drop associated with long-time soaking is due to partial closure of hydraulic fractures when a portion of the fluid was transported into cracks. They developed an analytical model of well productivity improvement for predicting the optimum soaking time. However, for propped fractures, their widths may not drop significantly during fluid soaking. We believe that the productivity drop after a long-soaking is due to the swelling of clayey minerals at the surfaces of cracks. Numerous papers have been published on the effects of clay swelling such as Anderson et al.'s (2010) study on the mechanism on clay swelling, Chuprin et al.'s (2022) paper on measuring swelling induced strain in heterogeneous shale samples, and Liu et al.'s (2022) study on permeability changes linked to clay swelling. However, due to the difficulty in quantitative description of the time-dependent swelling effect on well productivity, there is no method for predicting the optimum time of fluid soaking.

It is proposed in this study to predict the maximum time required for fluid to imbibe to the mid-point between two adjacent fractures along the crack. The midpoint between fractures is assumed to be the maximum distance a crack can propagate from a fracture as the crack will intersect another crack propagating from an adjacent fracture at the midpoint between the two fractures. This maximum time may serve as

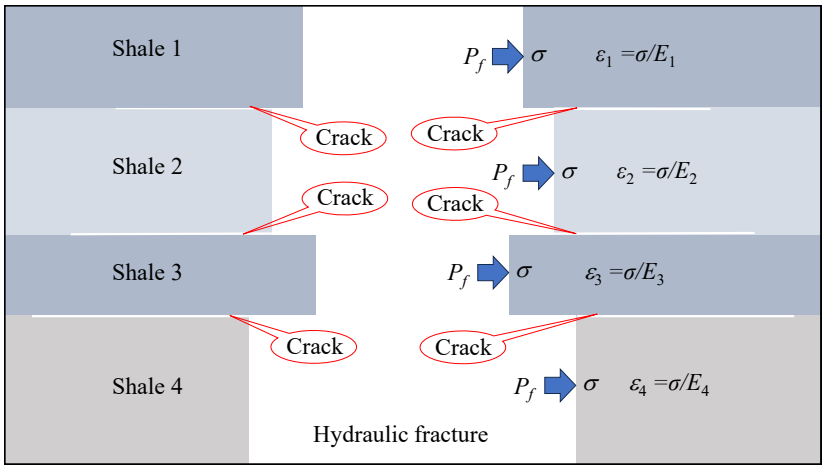

Fig. 3. Schematic to show the initiation of shale cracks induced by fracture pressure.

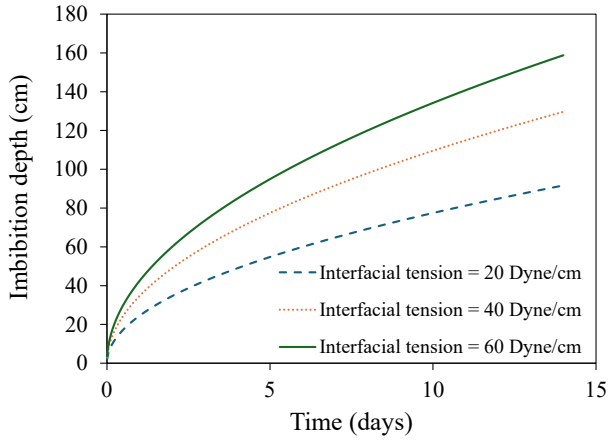

Fig. 4. Model-predicted spontaneous water imbibition into shale crack for different interfacial tensions.

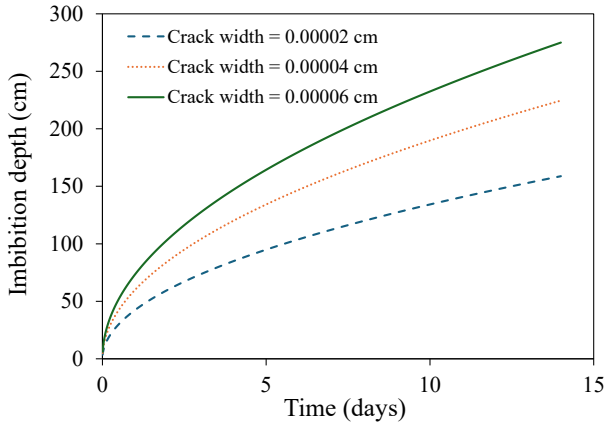

Fig. 6. Model-predicted spontaneous water imbibition into shale cracks for crack widths.

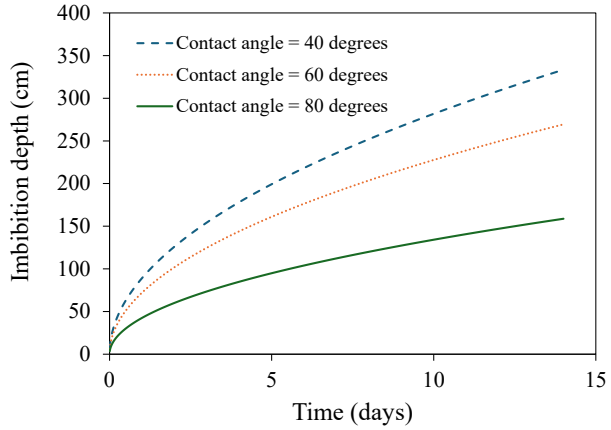

Fig. 5. Model-predicted spontaneous water imbibition into shale cracks for different contact angles.

the economic upper limit of soaking time in modern multi-fractured horizontal wells where fracture spacing is between 4 and 5 meters. Longer soaking times would not yield significant increase in well productivity.

Eq. (3) can be used for predicting the imbibition distance/depth along a crack with constant width. The challenge is the estimation of crack width. Another relation involving crack width is required to eliminate the crack width. Guo et al. (2020) proposed to use pressure fall off data obtained during fluid soaking to analyze imbibition rate in cracks. The dynamic imbibition rate (q_c) is expressed as:

$$q_c = \frac{c_f V_f}{n_f n_c} \frac{\mathrm{d}p}{\mathrm{d}t} \tag{5}$$

where c_f is compressibility of the wetting phase, V_f is the total supported fracture volume, n_f is the number of fractures which is assumed to be the number of perforation clusters, n_c is the number of cracks in each fracture, p is the average pressure in the fractures, and t is post-frac well shut-in time. The imbibition velocity in crack is expressed as:

$$v = \frac{c_f V_f}{w L_c n_f n_c} \frac{\mathrm{d}p}{\mathrm{d}t} \tag{6}$$

where L_c is the average crack length which is assumed to be equal to the average fracture length. Solving Eq. (6) for crack width gives:

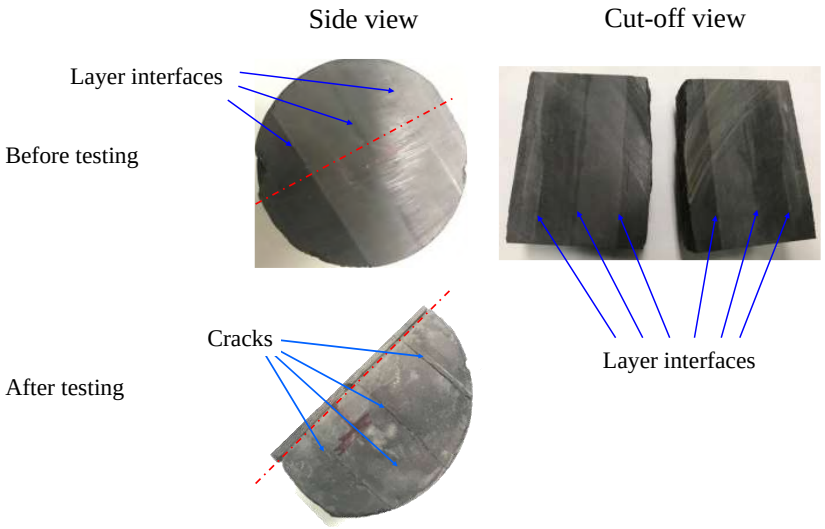

Fig. 7. Observed shale heterogeneities and cracks formed in lab-testing.

$$w = \frac{c_f V_f}{v L_c n_f n_c} \frac{\mathrm{d}p}{\mathrm{d}t} \tag{7}$$

Substituting Eq. (7) into Eq. (4) yields:

$$v = \sqrt{\frac{25 c_f V_f \sigma \cos\theta}{v L_c n_f n_c \mu_w t} \frac{\mathrm{d}p}{\mathrm{d}t}} \tag{8}$$

or:

$$v = \left(\frac{25 c_f V_f \sigma \cos\theta}{L_c n_f n_c \mu_w t} \frac{\mathrm{d}p}{\mathrm{d}t} \right)^{\frac{1}{3}} \tag{9}$$

which is rearranged to get:

$$\mathrm{d}x = \left(\frac{25 c_f V_f \sigma \cos\theta}{L_c n_f n_c \mu_w} \frac{\mathrm{d}p}{\mathrm{d}t} \right)^{\frac{1}{3}} t^{-\frac{1}{3}} \mathrm{d}t \tag{10}$$

which is integrated to result in:

$$x = \frac{3}{2} \left(\frac{25 c_f V_f \sigma \cos\theta}{L_c n_f n_c \mu_w} \frac{\mathrm{d}p}{\mathrm{d}t} \right)^{\frac{1}{3}} t^{\frac{2}{3}} \tag{11}$$

When the imbibition front reaches the mid-point between two adjacent fractures (S_f/2), the following equation holds:

$$\frac{S_f}{2} = \frac{3}{2} \left(\frac{25 c_f V_f \sigma \cos\theta}{L_c n_f n_c \mu_w} \frac{\mathrm{d}p}{\mathrm{d}t} \right)^{\frac{1}{3}} t_{\mathrm{end}}^{\frac{2}{3}} \tag{12}$$

which gives the ending time of soaking as follows:

$$t_{\mathrm{end}} = \frac{\left(\frac{S_f}{3} \right)^{\frac{3}{2}}}{\sqrt{\frac{25 c_f V_f \sigma \cos\theta}{L_c n_f n_c \mu_w} \frac{\mathrm{d}p}{\mathrm{d}t}}} \tag{13}$$

The major challenge in using this model is the determination of the number of cracks per fracture. It is suggested to estimate this quantity in labs where the shale cores are examined for shale heterogeneities and tested for crack formation. The principle is illustrated in Fig. 7. Detailed test procedure is shown in a previous work (Guo et al., 2020).

TMS is part of the Tuscaloosa Group, which was deposited along the northern Gulf of Mexico approximately 95-89 million years ago during the Cenomanian to Turonian stages of the late Upper Cretaceous (Lu et al., 2011). The Tuscaloosa Group represents the fifth transgressive-regressive cycle of the Cretaceous section, in which the TMS consists of the maximum-transgressive deposits (Liu, 2005). In the past few years, some efforts have been made to understand the characteristics of TMS. Allen Jr et al. (2014) investigated the structure, stratigraphy, and hydrocarbon distribution of the TMS trend in southwestern Mississippi. Lu et al. (2015) investigated the organic matter and oil generation in the TMS. Their experimental results showed that the core samples collected from the well Sun #1 Spinks contain 40% to 65% rich clay. The porosity measured was less than 4%, with permeability in the range of 10 to 79 nd. Besov et al. (2017) presented logging and laboratory petrophysical measurements of a TMS well. Hackley et al. (2018) reassessed the technically recoverable continuous resources of TMS. The mean resources of TMS are 1,537 million barrels of oil and 4,614 billion cubic feet of gas. Nippes (2019) investigated the production behavior of TMS wells in Mississippi. The EUR of 29 TMS wells in Mississippi using a minimum decline rate of 15% was between 60,964 and 714,704 barrels of oil. Guo and Yang (2019) analyzed the production data of 55 TMS wells. They mentioned that the long linear flow behavior of TMS wells is attributed to the ultralow permeability of the TMS. Borrok et al. (2019) analyzed the mineralogy and organic content of 11 TMS wells. They stated that most samples of TMS are characterized by a total clay content of 40 to 80 wt%, quartz of 20 to 40 wt%, and less than about 40 wt% calcite. Yang and Guo (2020) performed statistical analyses of reservoir and fracturing parameters using the production data of 16 TMS wells in Mississippi. The estimated permeability ranged from 53 to 210 nd. TMS development stopped in 2015 due to low oil price. It was recently planned to continue the development process. New multi-stage hydraulic fracturing technology will be used to reduce fracture spacing from about 20 meters to 4-6 meters. It is highly desirable to know the

Table 3. Fracture and fluid properties in the TMS (Guo et al., 2020).

Parameter	Value	Unit
Number of fractures per well (n_f)	102	-
Number of cracks per fracture (n_c)	7,200	-
Total fracturing fluid volume (V_f)	6,216,000	gal
Fracturing fluid compressibility (c_f)	0.000003	1/psi
The average crack length (L_c)	1,000	ft
Fracturing fluid interfacial tension (σ)	60	Dyne/cm
Fracturing fluid contact angle (θ)	80	degree
Fracturing fluid viscosity (μ_w)	1	cp

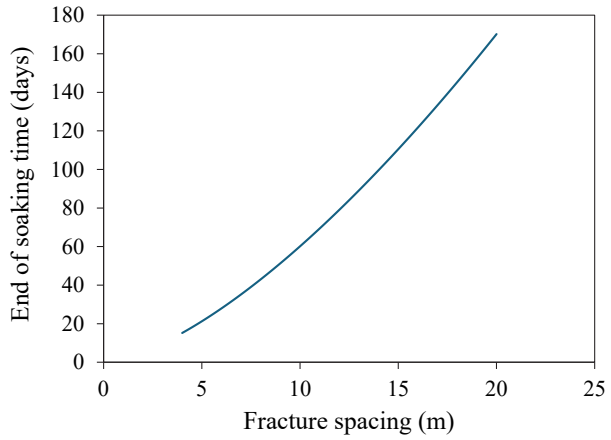

Fig. 8. Model-calculated soaking time when fluid imbibition front reaches the mid-point between two adjacent fractures.

optimum post-frac soaking time to improve well productivity.

Table 3 presents a list of typical parameter values relevant to soaking analysis for TMS well completion. The number of fractures per well is assumed to be the number of perforation clusters. The number of cracks per fracture was estimated in lab where the shale cores were examined for shale heterogeneities and tested for crack formation (Guo et al., 2020). Pressure fall-off data is not available in the TMS. Makhanov et al. (2013) recorded shut-in pressure for 25 hours to estimate water loss during shut-in periods. Because the data were measured for only 1 day, Guo et al. (2020) model-fitted the data and developed a correlation for extrapolation to a long-time period. The correlation takes the following form:

$$p_s = 4460t^{-0.044} \tag{14}$$

where the shut-in pressure p_s is in psi and shut-in time t is in hour. This correlation gives a pressure decline rate $\mathrm{d}p/\mathrm{d}t = 144$ psi/day approximately. Using this value and the data in Table 3, Eq. (13) allows for generating Fig. 8. This curve shows that the front of fluid imbibition should propagate 4 meters in 2 weeks and 6 meters in 4 weeks. These numbers should be considered as the optimum times of post-frac fluid imbibition.

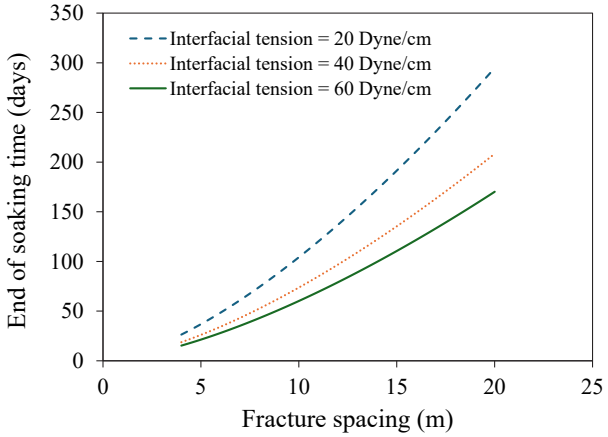

Fig. 9. Effect of interfacial tension on the soaking time when fluid imbibition front reaches the mid-point between two adjacent fractures.

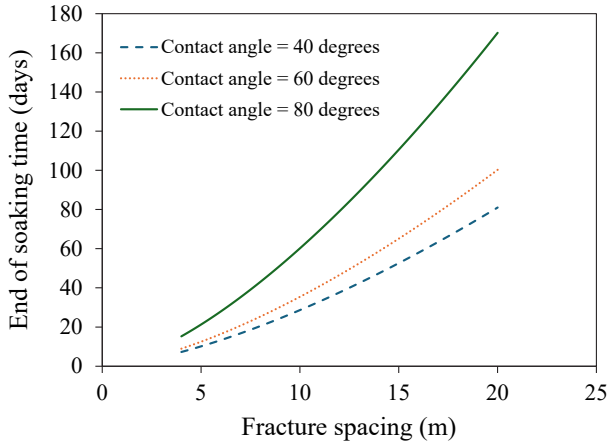

Fig. 10. Effect of contact angle on the soaking time when fluid imbibition front reaches the mid-point between two adjacent fractures.

Figs. 9-11 demonstrate a sensitivity analysis on the variables of interfacial tension, contact angle, and viscosity in the model. A general observation of the curve trends in these three figures is that the soaking time required for the fracturing fluid to imbibe to the mid-point between two adjacent fractures increases non-linearly with fracture spacing. In fact, Eq. (13) reveals that the required soaking time is proportional to the $3/2$ power of fracture spacing.

Fig. 9 presents the model-calculated effect of interfacial tension on the soaking time required for the fracturing fluid to imbibe to the mid-point between two adjacent fractures. The trends of curves in the figure indicate that increasing the liquid-shale interfacial tension can significantly shorten the soaking time. This is because interfacial tension is the driving force for spontaneous fluid imbibition. Fig. 9 also implies that the reduction in soaking time is not proportional to the interfacial tension in the range between 20 and 60 Dynes/cm. In fact, Eq. (13) reveals that the soaking time is inversely proportional to the square root of interfacial tension. Fig. 10 shows the model-calculated effect of contact angle on the soaking time required for the fracturing fluid to imbibe to the mid-point between two

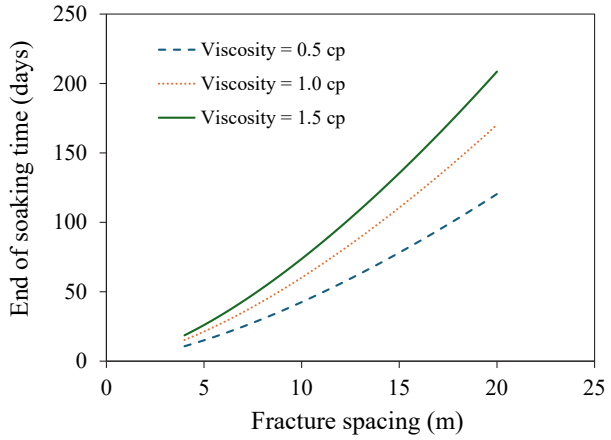

Fig. 11. Effect of fracturing fluid viscosity on the soaking time when fluid imbibition front reaches the mid-point between two adjacent fractures.

adjacent fractures. This is because contact angle controls the component of the interfacial force in the direction of fluid imbibition. Fig. 10 also shows that the reduction in soaking time is not proportional to the reduction in contact angle in the range between 40° and 80°. In fact, Eq. (13) reveals that the soaking time is inversely proportional to the square root of cosine of the contact angle. It implies that adding surfactants to the soaking fluid to increase contact angle will reduce soaking efficiency. Fig. 11 demonstrates the model-calculated effect of fracturing fluid viscosity on the soaking time required for the fracturing fluid to imbibe to the mid-point between two adjacent fractures. It suggests that reducing fluid viscosity can significantly enhance soaking efficiency. This is because fluid viscosity is a major factor affecting the resistance to fluid imbibition. This is why the use of slick water as friction reducer improved well productivity. Fig. 11 also shows that the reduction in soaking time is not proportional to the reduction in fluid viscosity in the range between 0.5 and 1.5 cp. In fact, Eq. (13) reveals that the soaking time is directly proportional to the square root of fluid viscosity.

4. Conclusions

Analytical solutions were developed in this study to describe spontaneous imbibition processes in shale matrix and shale cracks. The solution for shale crack was combined with pressure fall-off data to form a mathematical model for predicting the post-frac fluid soaking time required for the fluid to reach the mid-point between two adjacent hydraulic fractures. The following conclusions are drawn.

1) Spontaneous imbibition processes in shale matrix and shale cracks share the same governing equation. Its solutions for the two processes have the same form with parameters of different physical meanings. The imbibition distance is directly proportional to the square root of imbibition time. The imbibition velocity is inversely proportional to the square root of imbibition time.
2) The rate of spontaneous imbibition in shale cracks is much faster than that in shale matrix. Therefore, the optimum time for post-frac fluid soaking should be designed on the basis of the imbibition in shale cracks.
3) If the information of shale crack width is not known, pressure fall-off data needs to be recorded during a well soaking period. This information will enable the crack-imbibition model to predict the required fluid soaking time.
4) Case study with TMS data shows that the front of fluid imbibition should propagate 4 meters in 2 weeks and 6 meters in 4 weeks. These numbers should be considered as the optimum times of post-frac fluid imbibition if the shale swell effect is not significant. Future research should quantify the effects of shale swelling on spontaneous imbibition so that the information can be incorporated in the soaking model to fully describe the imbibition process for better prediction of well productivity.

Acknowledgements

The authors express their gratitude to the Energy Institute of Louisiana at the University of Louisiana at Lafayette for supporting the research.

Conflict of interest

The authors declare no competing interest.

References

Allen Jr., J. E., Meylan, M. A., Heitmuller, F. T. Determining hydrocarbon distribution using resistivity, Tuscaloosa Marine Shale, southwestern Mississippi. Gulf Coast Association of Geological Societies Transactions, 2014, 64: 41-57.

Anderson, R. L., Ratcliffe, I., Greenwell, H. C., et al. Clay swelling-a challenge in the oilfield. Earth-Science Reviews, 2010, 98(3-4): 201-216.

Besov, A., Tinni, A., Sondergeld, C., et al. Application of laboratory and field NMR to characterize the Tuscaloosa marine shale. Petrophysics, 2017, 58(3): 221-231.

Borrok, D. M., Yang, W., Wei, M., et al. Heterogeneity of the mineralogy and organic content of the Tuscaloosa Marine Shale. Marine and Petroleum Geology, 2019, 109: 717-731.

Cai, J. Some key issues and thoughts on spontaneous imbibition in porous media. Chinese Journal of Computational Physics, 2021, 38(5): 505-512. (in Chinese)

Cai, J., Perfect, E., Cheng, C. L., et al. Generalized modeling of spontaneous imbibition based on Hagen-Poiseuille flow in tortuous capillaries with variably shaped apertures. Langmuir, 2014, 30(18): 5142-5151.

Cai, J., Sun, S., Wang, H. Current advances in capillarity: Theories and applications. Capillarity, 2023, 7(2): 25-31.

Cai, J., Yu, B. Advances in studies of spontaneous imbibition in porous media. Advances in Mechanics, 2012, 42(6): 735-754. (in Chinese)

Chuprin, M., Naik Parrikar, P., Mokhtari, M., et al. Using digi-

tal image correlation for evaluating the impact of brine on swelling of heterogeneous shales. Rock Mechanics and Rock Engineering, 2022, 55(2): 1013-1035.

Crafton, J. W., Noe, S. L. Factors affecting early well productivity in six shale plays. Paper SPE 166101 Presented at the SPE Annual Technical Conference and Exhibition, New Orleans, Louisiana, 30 September-2 October, 2013.

Dutta, R., Lee, C., Odumabo, S., et al. Quantification of fracturing fluid migration due to spontaneous imbibition in fractured tight formations. Paper SPE 154939 Presented at the SPE Americas Unconventional Resources Conference, Pittsburgh, Pennsylvania, 5-7 June, 2012.

Ehlig-Economides, C. A., Economides, M. J. Water as proppant. Paper SPE 147603 Presented at the SPE Annual Technical Conference and Exhibition, Denver, Colorado, 30 October-2 November, 2011.

Guo, B., Shaibu, R., Hou, X. Crack propagation hypothesis and a model to calculate the optimum water-soaking period in shale gas/oil wells for maximizing well productivity. SPE Drilling & Completion, 2020, 35(4): 655-667.

Guo, B., Yang, X. Use of a new analytical model to match production data and identify opportunities to maximize well productivity in the Tuscaloosa Marine Shale reservoir. SPE Production & Operations, 2019, 34(4): 770-780.

Habibi, A., Binazadeh, M., Dehghanpour, H., et al. Advances in understanding wettability of tight oil formations. Paper SPE 175157 Presented at the SPE Annual Technical Conference and Exhibition, Houston, Texas, 28-30 September, 2015.

Hackley, P. C., Enomoto, C. B., Valentine, B. J., et al. Assessment of undiscovered continuous oil and gas resources in the Upper Cretaceous Tuscaloosa marine shale of the U.S. Gulf Coast, 2018. 2018-3043, 2018.

Handy, L. L. Determination of effective capillary pressures for porous media from imbibition data. Transactions of the AIME. 1960, 219(1): 75-80.

Kolodzie Jr., S. Analysis of pore throat size and use of the waxman-smits equation to determine OOIP in Spindle Field, Colorado. Paper SPE 9382 Presented at the SPE Annual Technical Conference and Exhibition, Dallas, Texas, 21-24 September, 1980.

Liu, B., Liang, Y., Ito, T. Numerical study on micro-cracks and permeability changes linked to clay swelling after fracturing in shale rock. Journal of Petroleum Science and Engineering, 2022, 217: 110847.

Liu, K. Upper cretaceous sequence stratigraphy, sea-level fluctuations, and oceanic anoxic events 2 and 3, northeastern Gulf of Mexico. Stratigraphy, 2005, 2(2): 147-166.

Lu, J., Milliken, K., Reed, R. M., et al. Diagenesis and sealing capacity of the middle Tuscaloosa mudstone at the Cranfield carbon dioxide injection site, Mississippi, USA. Environmental Geosciences, 2011, 18(1): 35-53.

Lu, J., Ruppel, S. C., Rowe, H. D. Organic matter pores and oil generation in the Tuscaloosa marine shale. AAPG Bulletin, 2015, 99(2): 333-357.

Makhanov, K., Dehghanpour, H., Kuru, E. Measuring liquid uptake of organic shales: A workflow to estimate water loss during shut-in periods. Paper SPE 167157 Presented at the SPE Unconventional Resources Conference Canada, Alberta, Canada, 5-7 November, 2013.

Nippes, V. Production behavior and decline curve analysis of Tuscaloosa Marine Shale wells in Wilkinson and Amite Counties, Mississippi. Lafayette, University of Louisiana at Lafayette, 2019.

Pittman, E. D. Relationship of porosity and permeability to various parameters derived from mercury injection-capillary pressure curves for sandstone. AAPG Bulletin, 1992, 76(2): 191-198.

Shaibu, R., Guo, B. The dilemma of soaking a hydraulically fractured horizontal shale well prior to flowback-a decade literature review. Journal of Natural Gas Science and Engineering, 2021, 94: 104084.

Shen, Y., Ge, H., Li, C., et al. Water imbibition of shale and its potential influence on shale gas recovery-a comparative study of marine and continental shale formations. Journal of Natural Gas Science and Engineering, 2016, 35: 1121-1128.

Wang, Q., Zhao, J., Hu, Y., et al. Shut-in time optimization after fracturing in shale oil reservoirs. Petroleum Exploration and Development, 2022, 49(3): 671-683.

Yaich, E., Williams, S., Bowser, A., et al. A case study: The impact of soaking on well performance in the Marcellus. Paper URTEC 2154766 Presented at the SPE/AAPG/SEG Unconventional Resources Technology Conference, San Antonio, Texas, 20-22 July, 2015.

Yan, Q., Lemanski, C., Karpyn, Z. T., et al. Experimental investigation of shale gas production impairment due to fracturing fluid migration during shut-in time. Journal of Natural Gas Science and Engineering, 2015, 24: 99-105.

Yang, X., Guo, B. Statistical analyses of reservoir and fracturing parameters for a multifractured shale oil reservoir in Mississippi. Energy Science & Engineering, 2020, 8(3): 616-626.

Appendix A. Mathematical modeling of spontaneous imbibition in porous media and cracks

Mass transfer in spontaneous imbibition processes is induced by capillary force. Mass transfer rate is reduced by viscous friction force and promoted or demoted by gravitational force, depending on orientation of the motion relative to gravity. Mass transfer processes in porous media and cracks without the effect of gravity (horizontal flow) are studied in this work.

Appendix A.1 Flow in porous media

The capillary force acting to the fluid over an area of porous media can be formulated based on interfacial tension, contact angle, perimeter of capillary, and porosity of porous media. It is customary to express the capillary force as a function of capillary pressure through a bulk area:

$$F_c = \varphi A p_c \tag{A1}$$

where F_c is capillary force in Dyne, φ is porosity in fraction, A is bulk area in cm^2, and p_c in capillary pressure in Dyne/cm^2. For a capillary having cross-section of equivalent circular shape with an equivalent radius, the capillary pressure is expressed as:

$$p_c = \frac{2\sigma\cos\theta}{r_c} \tag{A2}$$

where σ in interfacial tension in Dyne/cm, q is the contact angle measured in the wetting phase, and r_c is the equivalent capillary radius in cm.

The viscous friction force Ff acting on the porous area over an imbibition depth is expressed as:

$$F_f = A p_f \tag{A3}$$

where p_f is friction pressure in Dyne/cm^2.

For porous media, the frictional pressure can be expressed by Darcy's law as:

$$p_f = 981\frac{\mu_w v x}{k_{rw}k} \tag{A4}$$

where μ_w is wetting fluid viscosity in cp, v is velocity in cm/s, x is penetration of imbibition in cm, k_{rw} is the relative permeability to the wetting phase, and k is the absolution permeability in Darcy.

For horizontal imbibition processes where gravity effect is zero, applying Newton's second law of motion to the flowing fluid gives:

$$F_c - F_f = \rho\varphi A x\frac{\mathrm{d}v}{\mathrm{d}t} \tag{A5}$$

where ρ is fluid density in g/cc. Substitutions of Eqs. (A1) and (A3) into Eq. (A5) yield:

$$\varphi A\frac{2\sigma\cos\theta}{r_c} - 981A\frac{\mu_w v x}{k_{rw}k} = \rho\varphi A x\frac{\mathrm{d}v}{\mathrm{d}} \tag{A6}$$

which is simplified to yield:

$$\rho\varphi x\frac{\mathrm{d}v}{\mathrm{d}t} - \varphi\frac{2\sigma\cos\theta}{r_c} + 981\frac{\mu_w v x}{k_{rw}k} = 0 \tag{A7}$$

Because $v = \mathrm{d}x/\mathrm{d}t$, Eq. (A7) is rearranged to give:

$$\frac{\mathrm{d}^2x}{\mathrm{d}t^2} - \frac{2\sigma\cos\theta}{\rho r_c x} + 981\frac{\mu_w}{k_{rw}k\rho\varphi}\frac{\mathrm{d}x}{\mathrm{d}t} = 0 \tag{A8}$$

or:

$$\frac{\mathrm{d}^2x}{\mathrm{d}t^2} + a\frac{\mathrm{d}x}{\mathrm{d}t} + \frac{b}{x} = 0 \tag{A9}$$

where:

$$a = 981\frac{\mu_w}{k_{rw}k\rho\varphi} \tag{A10}$$

$$b = -\frac{2\sigma\cos\theta}{\rho r_c} \tag{A11}$$

Appendix A.2 Flow in cracks

The capillary force acting to the fluid over an inner area of a capillary tube can be formulated based on interfacial tension, contact angle, and perimeter of capillary. It is customary to express the capillary force as a function of capillary pressure:

$$F_c = Ap_c \tag{A12}$$

where F_c is capillary force in Dyne, A is the capillary inner area in cm^2, and p_c in capillary pressure in Dyne/cm^2. For a capillary with a rectangular cross-section, the capillary pressure is expressed as (Mahmood, 2024):

$$p_c = \frac{2\sigma\cos\theta}{hw}(h+w) \tag{A13}$$

where h and w are height and width of the rectangle. For a narrow crack where $w << h$, this equation us approximated by

$$p_c = \frac{2\sigma\cos\theta}{w} \tag{A14}$$

The viscous friction force F_f acting on the inner cross-sectional area of capillary is expressed as

$$F_f = Ap_f \tag{A15}$$

The frictional pressure loss p_f in capillary tube can be expressed as

$$p_f = \frac{f_f p v^2 x}{d_H} \tag{A16}$$

where f_f is friction factor, v is the average fluid velocity in cm/s, and d_H is hydraulic diameter of the capillary in cm. Assuming laminar flow the friction factor is expressed as

$$f_f = \frac{16}{N_{Re}} \tag{A17}$$

where the Reynolds number N_{Re} is given by

$$N_{Re} = \frac{100 d_H \rho v}{\mu_w} \tag{A18}$$

where μ_w is fluid viscosity in cp.

Substituting Eqs. (A17) and (A18) into Eq. (A16) gives:

$$p_f = \frac{16\mu_w v x}{100 d_H^2} \tag{A19}$$

For horizontal imbibition processes where gravity effect is zero, applying Newton's second law of motion to the flowing fluid gives:

$$F_c - F_f = \rho A x \frac{\mathrm{d}v}{\mathrm{d}t} \tag{A20}$$

Substitutions of Eqs. (A12) and (A15) into Eq. (A20) yield:

$$Ap_c - Ap_f = \rho A x \frac{\mathrm{d}v}{\mathrm{d}t} \tag{A21}$$

Substitutions of Eqs. (A19) into Eq. (A21) yield:

$$\frac{2\sigma\cos\theta}{w} - \frac{16\mu_w v x}{100 d_H^2} = \rho x \frac{\mathrm{d}v}{\mathrm{d}t} \tag{A22}$$

Because $v = \mathrm{d}x/\mathrm{d}t$, Eq. (A22) is rearranged to give:

$$\frac{\mathrm{d}^2 x}{\mathrm{d}t^2} + \frac{16\mu_w}{100\rho d_H^2}\frac{\mathrm{d}x}{\mathrm{d}t} - \frac{2\sigma\cos\theta}{w\rho x} = 0 \tag{A23}$$

or:

$$\frac{\mathrm{d}^2 x}{\mathrm{d}t^2} + a'\frac{\mathrm{d}x}{\mathrm{d}t} + \frac{b'}{x} = 0 \tag{A24}$$

where:

$$a' = \frac{16\mu_w}{100\rho d_H^2} \tag{A25}$$

$$b' = -\frac{2\sigma\cos\theta}{w\rho} \tag{A26}$$

Solution to Eq. (A9)(same as Eq. (A24)) was sought by Mahmood (2024) using the following initial conditions:

$$x = x_0 \quad \text{at} \quad t = 0 \tag{A27}$$

and:

$$\frac{\mathrm{d}x}{\mathrm{d}t} = v_0 \quad \text{at} \quad t = 0 \tag{A28}$$

The analytical solution takes a very complex form with singularity at the starting point. It was shown that the acceleration effect represented by second order derivative diminishes in a very short period. If the second order derivative term in Eq. (A9) is negligible, the governing equation degenerates to:

$$\frac{\mathrm{d}x}{\mathrm{d}t} + \frac{b}{ax} = 0 \tag{A29}$$

which takes an integration form of:

$$\int_0^x x\mathrm{d}x = -\frac{b}{a}\int_0^t \mathrm{d}t \tag{A30}$$

which is integrated to yield:

$$x = \sqrt{-\frac{2b}{a}t} \tag{A31}$$

Substituting Eqs. (A10) and (A11) into Eq. (A31) results in a solution for imbibition in porous media:

$$x = \sqrt{\frac{\sigma k_{rw} k\varphi\cos\theta}{245.25\mu_w r_c}t} \tag{A32}$$

Substituting Eqs. (A25) and (A26) into Eq. (A31) results in a solution for imbibition in cracks:

$$x = \sqrt{\frac{25d_H^2\sigma\cos\theta}{\mu_w w}t} \tag{A33}$$

Because the hydraulic diameter of crack is approximately equal to $2w$, Eq. (A22) becomes

$$x = \sqrt{\frac{100w\sigma\cos\theta}{\mu_w}t} \tag{A34}$$

References

Mahmood, M. Dynamic mass transfer in oil well cement cracks. Lafayette, University of Louisiana at Lafayette, 2024.